Nitrogen isotope fractionation during gas-to-particle conversion of NO_x to NO_3^- in the atmosphere – implications for isotope-based NO_x source apportionment

Yunhua Chang[1, 2, 3], Yanlin Zhang[1, 2, 3*], Chongguo Tian[4], Shichun Zhang[5], Xiaoyan Ma[6], Fang Cao[1, 2, 3], Xiaoyan Liu[1, 2, 3], Wenqi Zhang[1, 2, 3], Thomas Kuhn[7], and Moritz F. Lehmann[7]

[1]Yale-NUIST Center on Atmospheric Environment, International Joint Laboratory on Climate and Environment Change (ILCEC), Nanjing University of Information Science & Technology, Nanjing 210044, China

[2]Key Laboratory of Meteorological Disaster, Ministry of Education (KLME)/ Collaborative Innovation Center on Forecast and Evaluation of Meteorological Disasters (CIC-FEMD), Nanjing University of Information Science & Technology, Nanjing 210044, China

[3]Jiangsu Provincial Key Laboratory of Agricultural Meteorology, College of Applied Meteorology, Nanjing University of Information Science & Technology, Nanjing 210044, China

[4]Key Laboratory of Coastal Environmental Processes and Ecological Remediation, Yantai Institute of Coastal Zone Research, Chinese Academy of Sciences, Yantai 264003, China

[5]Northeast Institute of Geography and Agroecology, Chinese Academy of Sciences, 4888 Shengbei Road, Changchun 130102, China

[6]Key Laboratory for Aerosol Cloud-Precipitation of China Meteorological Administration, Earth System Modeling Center, Nanjing University of Information Science and Technology, Nanjing 10044, China

[7]Aquatic and Isotope Biogeochemistry, Department of Environmental Sciences, University of Basel, Basel 4056, Switzerland

[*] Corresponding author: Yanlin Zhang

E-mail address: dryanlinzhang@outlook.com

Abstract

Atmospheric fine-particle (PM$_{2.5}$) pollution is frequently associated with the formation of particulate nitrate (pNO$_3^-$), the end product of the oxidation of NO$_x$ gases (=NO+NO$_2$) in the upper troposphere. The application of stable nitrogen (N) (and oxygen) isotope analyses of pNO$_3^-$ to constrain NO$_x$ source partitioning in the atmosphere requires the knowledge of the isotope fractionation during the reactions leading to nitrate formation. Here we determined the δ^{15}N values of fresh pNO$_3^-$ (δ^{15}N-pNO$_3^-$) in PM$_{2.5}$ at a rural site in Northern China, where atmospheric pNO$_3^-$ can be attributed exclusively to biomass burning. The observed δ^{15}N-pNO$_3^-$ (12.17±1.55‰; n=8) was much higher than the N isotopic source signature of NO$_x$ from biomass burning (1.04±4.13‰). The large difference between δ^{15}N-pNO$_3^-$ and δ^{15}N-NO$_x$ ($\Delta(\delta^{15}$N)) can be reconciled by the net N isotope effect (ε_N) associated with the gas-particle conversion from NO$_x$ to NO$_3^-$. For the biomass-burning site, a mean ε_N ($\approx \Delta(\delta^{15}$N)) of 10.99±0.74‰ was assessed through a newly-developed computational quantum chemistry (CQC) module. ε_N depends on the relative importance of the two dominant N isotope exchange reactions involved (NO$_2$ reaction with OH versus hydrolysis of dinitrogen pentoxide (N$_2$O$_5$) with H$_2$O), and varies between regions, and on a diurnal basis. A second, slightly higher CQC-based mean value for ε_N (15.33±4.90‰) was estimated for an urban site with intense traffic in Eastern China, and integrated in a Bayesian isotope mixing model to make isotope-based source apportionment estimates for NO$_x$ at this site. Based on the δ^{15}N values (10.93±3.32‰, n=43) of ambient pNO$_3^-$ determined for the urban site, and considering the location-specific estimate for ε_N, our results reveal that the relative contribution of coal combustion and road traffic to urban NO$_x$ are 32±11% and 68±11%,

respectively. This finding agrees well with a regional bottom-up emission inventory of NO$_x$. Moreover, the variation pattern of OH contribution to ambient pNO$_3^-$ formation calculated by the CQC module is consistent with that simulated by the Weather Research and Forecasting model coupled with Chemistry (WRF-Chem), further confirming the robustness of our estimates. Our investigations also show that, without the consideration of the N isotope effect during pNO$_3^-$ formation, the observed δ^{15}N-pNO$_3^-$ at the study site would erroneously imply that NO$_x$ is derived almost entirely from coal combustion. Similarly, reanalysis of reported δ^{15}N-NO$_3^-$ data throughout China and its neighboring areas suggests that NO$_x$ emissions from coal combustion may be substantively overestimated (by >30%) when the N isotope fractionation during atmospheric pNO$_3^-$ formation is neglected.

1 Introduction

Nitrogen oxides (NO$_x$ = NO + NO$_2$) are among the most important molecules in tropospheric chemistry. They are involved in the formation of secondary aerosols and atmospheric oxidants, such as ozone (O$_3$) and hydroxyl radicals (OH), which controls the self-cleansing capacity of the atmosphere (Galloway et al., 2003; Seinfeld and Pandis, 2012; Solomon et al., 2007). The sources of NO$_x$ include both anthropogenic and natural origins, with more than half of the global burden ($\sim$40 Tg N yr^{-1}) currently attributed to fossil fuel burning (22.4-26.1 Tg N yr^{-1}) and the rest primarily derived from nitrification/denitrification in soils (including wetlands; 8.9 $\pm$ 1.9 Tg N yr^{-1}), biomass burning (5.8 $\pm$ 1.8 Tg N yr^{-1}), lightning (2-6 Tg N yr^{-1}), and oxidation of N$_2$O in the stratosphere (0.1-0.6 Tg N yr^{-1}) (Jaegle et al., 2005; Richter et al., 2005; Lamsal et al., 2011; Price et al., 1997; Yienger and Levy, 1995; Miyazaki et al., 2017; Duncan et al., 2016; Anenberg et al., 2017; Levy et al., 1996). The main/ultimate sinks for NO$_x$ in the troposphere are the oxidation to nitric acid (HNO$_{3(g)}$) and the formation of aerosol-phase particulate nitrate (pNO$_3^-$) (Seinfeld and Pandis, 2012), the partitioning of which may vary on diurnal and seasonal time scales (Morino et al., 2006).

Emissions of NO$_x$ occur mostly in the form of NO (Seinfeld and Pandis, 2012; Leighton,

80   1961). During daytime, transformation from NO to NO_2 is rapid (few minutes) and

81   proceeds in a photochemical steady state, controlled by the oxidation of NO by O_3 to

82   NO_2, and the photolysis of NO_2 back to NO (Leighton, 1961):

83   (R1) $NO + O_3 \longrightarrow NO_2 + O_2$

84   (R2) $NO_2 + hv \longrightarrow NO + O$

85   (R3) $O + O_2 \xrightarrow{M} O_3,$
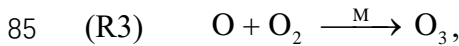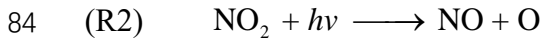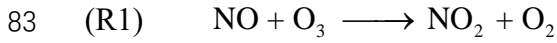
86   where M is any non-reactive species that can take up the energy released to stabilize

87   O. NO_x oxidation to HNO_3 is governed by the following equations. During daytime:

88   (R4) $NO_2 + OH \xrightarrow{M} HNO_3,$
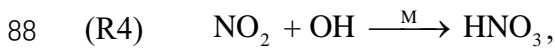
89   and during nighttime:

90   (R5) $NO_2 + O_3 \longrightarrow NO_3 + O_2$

91   (R6) $NO_3 + NO_2 \xrightarrow{M} N_2O_5$

92   (R7) $N_2O_5 + H_2O_{(surface)} \xrightarrow{aerosol} 2HNO_3.$
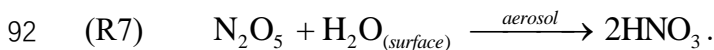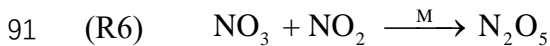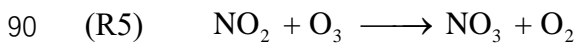
93   HNO_3 then reacts with gas-phase NH_3 to form ammonium nitrate (NH_4NO_3) aerosols.

94   If the ambient relative humidity (RH) is lower than the efflorescence relative humidity

95   (ERH) or crystallization relative humidity (CRH), solid-phase $NH_4NO_3(s)$ is formed

96   (Smith et al., 2012; Ling and Chan, 2007):

97   (R8a) $NH_4NO_3 \rightleftharpoons HNO_3(g) + NH_3(g).$
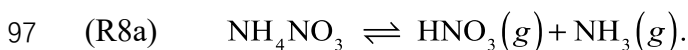
98   If ambient RH exceeds the ERH or CRH, HNO_3 and NH_3 dissolve into the aqueous

99   phase (aq) (Smith et al., 2012; Ling and Chan, 2007):

100   (R8b) $HNO_3(g) + NH_3(g) \rightleftharpoons NO_3^-(aq) + NH_4^+(aq).$

101 Whilst global NO_x emissions are well constrained, individual source attribution and

102 their local or regional role in particulate nitrate formation are difficult to assess due to

103 the short lifetime of NO_x (typically less than 24 hr), and the high degree of

104 spatiotemporal heterogeneity with regards to the ratio between gas-phase HNO_3 and

105 particulate NO_3^- (pNO_3^-) (Duncan et al., 2016; Lu et al., 2015; Zong et al., 2017; Zhang

106 et al., 2003). Given the conservation of the nitrogen (N) atom between NO_x sources and

107 sinks, the N isotopic composition of pNO_3^- can be related to the different origins of the

108 emitted NO_x, and thus provides valuable information on the partitioning of the NO_x

109 sources (Morin et al., 2008). Such N isotope balance approach works best if the N

110 isotopic composition of various NO_x sources display distinct $^{15}N/^{14}N$ ratios (reported

111 as $\delta^{15}N = \dfrac{\left(^{15}N/^{14}N\right)_{sample} - \left(^{15}N/^{14}N\right)_{N_2}}{\left(^{15}N/^{14}N\right)_{N_2}} \times 1000$). The $\delta^{15}N\text{-}NO_x$ of coal-fired power

112 plant (+10‰ to +25‰) (Felix et al., 2012; Heaton, 1990; Felix et al., 2013), vehicle

113 (+3.7‰ to +5.7‰) (Heaton, 1990; Walters et al., 2015; Felix and Elliott, 2014; Felix et

114 al., 2013; Wojtal et al., 2016), and biomass burning (-7‰ to +12‰) emissions (Fibiger

115 and Hastings, 2016), for example, are generally higher than that of lightning (-0.5‰ to

116 +1.4‰) (Hoering, 1957) and biogenic soil (-48.9‰ to -19.9‰) emissions (Li and Wang,

117 2008; Felix and Elliott, 2014; Felix et al., 2013), allowing the use of isotope mixing

118 models to gain insight on the NO_x source apportionment for gases, aerosols, as well as

119 the resulting nitrate deposition (-15‰ to +15‰) (Elliott et al., 2007; Zong et al., 2017;

120 Savarino et al., 2007; Morin et al., 2008; Elliott et al., 2009; Park et al., 2018; Altieri et

121 al., 2013; Gobel et al., 2013). In addition, because of mass-independent fractionation

122 during its formation (Thiemens, 1999; Thiemens and Heidenreich, 1983), ozone

123 possesses a strong isotope anomaly ($\Delta^{17}O \approx \delta^{17}O - 0.52*\delta^{18}O$), which is propagated into

124 the most short-lived oxygen-bearing species, including NO_x and nitrate. Therefore, the

125 oxygen isotopic composition of nitrate ($\delta^{18}O$, $\Delta^{17}O$) can provide information on the

126 oxidants involved in the conversion of NO_x to nitrate (Michalski et al., 2003; Geng et

127 al., 2017). Knopf et al. (2006, 2011) and Shiraiwa et al. (2012) have shown that NO_3

128 can be taken up efficiently by organic (e.g., levoglucosan) aerosol and may dominate

129 oxidation of aerosol in the polluted urban nighttime (Kaiser et al., 2011). Globally,

130 theoretical modeling results show that nearly 76%, 18%, and 4% of annual inorganic

131 nitrate are formed via pathways/reactions involving OH, N_2O_5, and dimethylsulfide

132 (DMS) or hydrocarbons (HC), respectively (e.g., Alexander et al., 2009). The stable O

133 isotopic composition of atmospheric nitrate is a powerful proxy for assessing which

134 oxidation pathways are important for converting NO_x into nitrate under changing

135 environmental conditions (e.g., polluted, volcanic events, climate change). In the same

136 line, in this study, the average $\delta^{18}O$ value of pNO_3^- in Nanjing City was 83.0 ± 11.2‰

137 (see discussion later), suggesting that pNO_3^- formation is dominated by the pathways

138 of "OH + NO_2" and the heterogeneous hydrolysis of N_2O_5.

139 $\delta^{15}N$-based source apportionment of NO_x requires knowledge of how kinetic and

140 equilibrium isotope fractionation may impact $\delta^{15}N$ values during the conversion of NO_x

141 to nitrate (Freyer, 1978; Walters et al., 2016). If these isotope effects are considerable,

142 they may greatly limit the use of $\delta^{15}N$ values of pNO_3^- for NO_x source partition (Walters

143 et al., 2016). Previous studies didn't take into account the potentially biasing effect of

144 N isotope fractionation, because they assumed that changes in the $\delta^{15}N$ values during

145 the conversion of NO_x to nitrate are minor (without detailed explanation) (Kendall et

146 al., 2007; Morin et al., 2008; Elliott et al., 2007) or relatively small (e.g., +3‰) (Felix

147 and Elliott, 2014; Freyer, 2017). However, a field study by Freyer et al. (1993) has

148 indicated that N isotope exchange may have a strong influence on the observed $\delta^{15}N$

149 values in atmospheric NO and NO_2, implying that isotope equilibrium fractionation

150 may play a significant role in shaping the $\delta^{15}N$ of NO_y species (the family of oxidized

151 nitrogen molecules in the atmosphere, including NO_x, NO_3, NO_3^-, peroxyacetyl nitrate

152 etc.). The transformation of NO_x to nitrate is a complex process that involves several

153 different reaction pathways (Walters et al., 2016). To date, few fractionation factors for

154 this conversion have been determined. Recently, Walters and Michalski (2015) and

155 Walters et al. (2016) used computational quantum chemistry methods to calculate N

156 isotope equilibrium fractionation factors for the exchange between major NO_y

157 molecules and confirmed theoretical predictions that ^{15}N isotopes enrich in the more

158   oxidized form of NO_y, and that the transformation of NO_x to atmospheric nitrate (HNO_3,

159   NO_3 (aq), NO_3 (g)) continuously increases the $\delta^{15}N$ in the residual NO_x pool.

160   As a consequence of its severe atmospheric particle pollution during the cold season,

161   China has made great efforts toward reducing NO_x emissions from on-road traffic (e.g.,

162   improving emission standards, higher gasoline quality, vehicle travel restrictions) (Li

163   et al., 2017). Moreover, China has continuously implemented denitrogenation

164   technologies (e.g., selective catalytic reduction or SCR) in the coal-fired power plants

165   sector since the mid-2000s, and has been phasing out small inefficient units (Liu et al.,

166   2015). Monitoring and assessing the efficiency of such mitigation measures, and

167   optimizing policy efforts to further reduce NO_x emissions, requires knowledge of the

168   vehicle- and power plant-emitted NO_x to particulate nitrate in urban China (Ji et al.,

169   2015; Fu et al., 2013; Zong et al., 2017). In this study, the chemical components of

170   ambient fine particles ($PM_{2.5}$) were quantified, and the isotopic composition of

171   particulate nitrate ($\delta^{15}N\text{-}NO_3^-$, $\delta^{18}O\text{-}NO_3^-$) was assessed in order to elucidate ambient

172   NO_x sources in Nanjing City of Eastern China. We also investigated the potential

173   isotope effect during the formation of nitrate aerosols from NO_x, and evaluated how

174   disregard of such N isotope fractionation can bias N-isotope mixing model-based

175   estimates on the NO_x source apportionment for nitrate deposition.

176   **2 Methods**

177   **2.1 Field sampling**

178   In this study, $PM_{2.5}$ aerosol samples were collected on precombusted (450 °C for 6 hr)

179   quartz filters (25 × 20 cm) on a day/night basis, using high-volume air samplers at a

180   flow rate of 1.05 m^3 min^{-1} in Sanjiang and Nanjing (Fig. 1). After sampling, the filters

181   were wrapped in aluminum foil, packed in air-tight polyethylene bags and stored at -

182   20 °C prior to further processing and analysis. Four blank filters were also collected.

183   They were exposed for 10 min to ambient air (i.e., without active sampling). $PM_{2.5}$ mass

184   concentration was analyzed gravimetrically (Sartorius MC5 electronic microbalance)

185   with a $\pm$ 1 μg precision before and after sampling (at 25°C and 45 $\pm$ 5% during

186   weighing).

187

188   **Figure 1.**

189

190   The Sanjiang campaign was performed during a period of intensive burning of

191   agricultural residues between October 8 and 18, 2013, to examine if there is any

192   significant difference between the δ^{15}N values of pNO$_3^-$ and NO$_x$ emitted from biomass

193   burning. The Sanjiang site (in the following abbreviated as SJ; 47.35°N, 133.31°E) is

194   located at an ecological experimental station affiliated with the Chinese Academy of

195   Sciences located in the Sanjiang Plain, a major agricultural area predominantly run by

196   state farms in Northeastern China (Fig. 1). Surrounded by vast farm fields and bordering

197   Far-Eastern Russia, SJ is situated in a remote and sparsely populated region, with a

198   harsh climate and rather poorly industrialized economy. The annual mean temperature

199   at SJ is close to the freezing point, with daily minima ranging between -31 and -15°C

200   in the coldest month January. As a consequence of the relatively low temperatures (also

201   during summer), biogenic production of NO$_x$ through soil microbial processes is rather

202   weak. SJ is therefore an excellent environment where to collect biomass burning-

203   emitted aerosols with only minor influence from other sources.

204   The Nanjing campaign was conducted between 17 December 2014 and 8 January 2015

205   with the main objective to examine whether N isotope measurements can be used as a

206   tool to elucidate NO$_x$ source contributions to ambient pNO$_3^-$ during times of severe

207   haze. Situated in the lower Yangtze River region, Nanjing is, after Shanghai, the second

208   largest city in Eastern China. The aerosol sampler was placed at the rooftop of a building

209   on the Nanjing University of Information Science and Technology campus (in the

210   following abbreviated as NJ; 18 m a.g.l.; 32.21° N, 118.72° E; Fig. 1), where NO$_x$

211   emissions derive from both industrial and transportation sources.

2.2 Laboratory analysis

The mass concentrations of inorganic ions (including SO_4^{2-}, NO_3^-, Cl^-, NH_4^+, K^+, Ca^{2+}, Mg^{2+}, and Na^+), carbonaceous components (organic carbon or OC, elemental carbon or EC), and water-soluble organic carbon or WSOC were determined using an ion chromatograph (761 Compact IC, Metrohm, Switzerland), a thermal/optical OC/EC analyzer (RT-4 model, Sunset Lab. Inc., USA), and a TOC analyzer (Shimadzu, TOC-VCSH, Japan), respectively. Importantly, levoglucosan, a molecular marker for the biomass combustion aerosols was detected using a Dionex^{TM} ICS-5000$^+$ system (Thermo Fisher Scientific, Sunnyvale, USA). Chemical aerosol analyses, including sample pre-treatment, analytical procedures, protocol adaption, detection limits, and experimental uncertainty were described in detail in our previous work (Cao et al., 2016; Cao et al., 2017).

For isotopic analyses of aerosol nitrate, aerosol subsamples were generated by punching 1.4-cm disks out of the filters. In order to extract the NO_3^-, sample discs were placed in acid-washed glass vials with 10 ml deionized water and placed in an ultra-sonic water bath for 30 min. Between one and four disks were used for NO_x extraction, dependent on the aerosol NO_3^- content on the filters, which was determined independently. The extracts were then filtered (0.22 μm) and analyzed the next day. N and O isotope analyses of the extracted/dissolved aerosol nitrate ($^{15}N/^{14}N$, $^{18}O/^{16}O$) were performed using the denitrifier method (Sigman et al., 2001; Casciotti et al., 2002). Briefly, sample NO_3^- is converted to nitrous oxide (N_2O) by denitrifying bacteria that lack N_2O reductase activity (*Pseudomonas chlororaphis* ATCC# 13985; formerly *Pseudomonas aureofaciens*, referred to below as such). N_2O is extracted, purified, and analyzed for its N and O isotopic composition using a continuous-flow isotope ratio mass spectrometer (Thermo Finnigan Delta$^+$, Bremen, German). Nitrate N and O isotope ratios are reported in the conventional δ-notation with respect to atmospheric N_2 and standard mean ocean water (V-SMOW) respectively. Analyses are calibrated using the international nitrate isotope standard IAEA-N3, with a $\delta^{15}N$ value of 4.7‰ and a $\delta^{18}O$

value of 25.6‰ (Böhlke et al., 2003). The blank contribution was generally lower than 0.2 nmol (as compared to 20 nmol of sample N). Based on replicate measurements of standards and samples, the analytical precision for $\delta^{15}N$ and $\delta^{18}O$ was generally better than ± 0.2‰ and ± 0.3‰ (1σ), respectively.

The denitrifier method generates $\delta^{15}N$ and $\delta^{18}O$ values of the combined pool of NO_3^- and NO_2^-. The presence of substantial amounts of NO_2^- in NO_3^- samples may lead to errors with regards to the analysis of $\delta^{18}O$ (Wankel et al., 2010). We refrained from including a nitrite-removal step, because nitrite concentrations in our samples were always < 1% of the NO_3^- concentrations. In the following $\delta^{15}N_{NOx}$ and $\delta^{18}O_{NOx}$ are thus referred to as nitrate $\delta^{15}N$ and $\delta^{18}O$ (or $\delta^{15}N_{NO3}$ and $\delta^{18}O_{NO3}$).

In the case of atmospheric/aerosol nitrate samples with comparatively high $\delta^{18}O$ values, $\delta^{15}N$ values tend to be overestimated by 1-2‰ (Hastings et al., 2003), if the contribution of $^{14}N^{14}N^{17}O$ to the N_2O mass 45 signal is not accounted for during isotope ratio analysis. For most natural samples, the mass-dependent relationship can be approximated as $\delta^{17}O \approx 0.52 \times \delta^{18}O$, and the $\delta^{18}O$ can be used for the ^{17}O correction. Atmospheric NO_3^- does not follow this relationship but inhabits a mass-independent component. Thus, we adopted a correction factor of 0.8 instead of 0.52 for the ^{17}O to ^{18}O linearity (Hastings et al., 2003).

2.3 Calculation of N isotope fractionation value (ε_N)

As we described above, the transformation process of NO_x to HNO_3/NO_3^- involves multiple reaction pathways (see also Fig. S1) and is likely to undergo isotope equilibrium exchange reactions. The measured $\delta^{15}N-NO_3^-$ values of aerosol samples are thus reflective of the combined N isotope signatures of various NO_x sources ($\delta^{15}N-NO_x$) plus any given N isotope fractionation. Recently, Walter and Michalski (2015) used a computational quantum chemistry approach to calculate isotope exchange fractionation factors for atmospherically relevant NO_y molecules, and based on this approach, Zong et al. (2017) estimated the N isotope fractionation during the transformation of NO_x to

267 $p\text{NO}_3^-$ at a regional background site in China. Here we adopt, and slightly modify, the

268 approach by Walter and Michalski (2015) and Zong et al. (2017), and assumed that the

269 net N isotope effect ε_N (for equilibrium processes A↔B: $\varepsilon_{A\leftrightarrow B} =$

270 $\left(\dfrac{(\text{heavy isotope/light isotope})_A}{(\text{heavy isotope/light isotope})_B} - 1 \right) \bullet 1000‰$; ε_N refers to $\varepsilon_{N(NO_x \leftrightarrow pNO_3^-)}$ in this

271 study unless otherwise specified) during the gas-to-particle conversion from NO_x to

272 $p\text{NO}_3^-$ formation ($\Delta\left(\delta^{15}\text{N}\right)_{pNO_3^- - NO_x} = \delta^{15}\text{N-}p\text{NO}_3^- - \delta^{15}\text{N-NO}_x \approx \varepsilon_N$) can be considered

273 a hybrid of the isotope effects of two dominant N isotopic exchange reactions:

$$\begin{aligned}\varepsilon_N &= \gamma \times \varepsilon_{N\left(NO_x \leftrightarrow pNO_3^-\right)_{OH}} + \left(1-\gamma\right) \times \varepsilon_{N\left(NO_x \leftrightarrow pNO_3^-\right)_{H_2O}} \\ &= \gamma \times \varepsilon_{N\left(NO_x \leftrightarrow HNO_3\right)_{OH}} + \left(1-\gamma\right) \times \varepsilon_{N\left(NO_x \leftrightarrow HNO_3\right)_{H_2O}}\end{aligned} \qquad (1)$$

275 where γ represents the contribution from isotope fractionation by the reaction of NO_x

276 and photo-chemically produced OH to form HNO_3 (and $p\text{NO}_3^-$), as shown by

277 $\varepsilon_{N\left(NO_x \leftrightarrow HNO_3\right)_{OH}}$ ($\varepsilon_{N\left(NO_x \leftrightarrow pNO_3^-\right)_{OH}}$). The remainder is formed by the hydrolysis of N_2O_5

278 with aerosol water to generate HNO_3 (and $p\text{NO}_3^-$), namely, $\varepsilon_{N\left(NO_x \leftrightarrow HNO_3\right)_{H_2O}}$

279 ($\varepsilon_{N\left(NO_x \leftrightarrow pNO_3^-\right)_{H_2O}}$). Assuming that kinetic N isotope fractionation associated with the

280 reaction between NO_x and OH is negligible, $\varepsilon_{N\left(NO_x \leftrightarrow pNO_3^-\right)_{OH}}$ can be calculated based on

281 mass-balance considerations:

$$\begin{aligned}\varepsilon_{N\left(NO_x \leftrightarrow pNO_3^-\right)_{OH}} &= \varepsilon_{N\left(NO_x \leftrightarrow HNO_3\right)_{OH}} = \varepsilon_{N\left(NO_2 \leftrightarrow HNO_3\right)_{OH}} \\ &= 1000 \times \left[\frac{\left(^{15}\alpha_{NO_2/NO} - 1\right)\left(1 - f_{NO_2}\right)}{\left(1 - f_{NO_2}\right) + \left(^{15}\alpha_{NO_2/NO} \times f_{NO_2}\right)} \right]\end{aligned} \qquad (2)$$

283 where $^{15}\alpha_{NO_2/NO}$ is the temperature-dependent (see equation 7 and Table S1)

284 equilibrium N isotope fractionation factor between NO_2 and NO, and f_{NO_2} is the

285 fraction of NO_2 in the total NO_x. f_{NO_2} ranges from 0.2 to 0.95 (Walters and

286 Michalski, 2015). Similarly, assuming a negligible kinetic isotope fractionation

287 associated with the reaction $N_2O_5 + H_2O + aerosol \rightarrow 2HNO_3$, $\varepsilon_{N\left(NO_x \leftrightarrow pNO_3^-\right)_{H_2O}}$ can be

288 computed from the following equation:

$$\varepsilon_{N\left(NO_x \leftrightarrow pNO_3^-\right)_{H_2O}} = \varepsilon_{N\left(NO_x \leftrightarrow HNO_3\right)_{H_2O}} =$$
$$\varepsilon_{N\left(NO_x \leftrightarrow N_2O_5\right)_{H_2O}} = 1000 \times \left(^{15}\alpha_{N_2O_5/NO_2} - 1\right) \qquad (3)$$

290 where $^{15}\alpha_{N_2O_5/NO_2}$ is the equilibrium isotope fractionation factor between N_2O_5 and

291 NO_2, which also is temperature-dependent (see equation 7 and Table S1).

292 Following Walter and Michalski (2015) and Zhong et al. (2017), γ can then be

293 approximated based on the O isotope fractionation during the conversion of NO_x to

294 pNO_3^-:

$$\varepsilon_{O\left(NO_x \leftrightarrow pNO_3^-\right)} = \gamma \times \varepsilon_{O\left(NO_x \leftrightarrow pNO_3^-\right)_{OH}} + \left(1 - \gamma\right) \times \varepsilon_{O\left(NO_x \leftrightarrow pNO_3^-\right)_{H_2O}}$$
$$= \gamma \times \varepsilon_{O\left(NO_x \leftrightarrow HNO_3\right)_{OH}} + \left(1 - \gamma\right) \times \varepsilon_{O\left(NO_x \leftrightarrow HNO_3\right)_{H_2O}} \qquad (4)$$

296 where $\varepsilon_{O\left(NO_x \leftrightarrow pNO_3^-\right)_{OH}}$ and $\varepsilon_{O\left(NO_x \leftrightarrow pNO_3^-\right)_{H_2O}}$ represent the O isotope effects associated

297 with pNO_3^- generation through the reaction of NO_x and OH to form HNO_3, and the

298 hydrolysis of N_2O_5 on a wetted surface to form HNO_3, respectively. $\varepsilon_{O\left(NO_x \leftrightarrow pNO_3^-\right)_{OH}}$ can

299 be further expressed as:

$$\varepsilon_{O\left(NO_x \leftrightarrow pNO_3^-\right)_{OH}} = \varepsilon_{O\left(NO_x \leftrightarrow HNO_3\right)_{OH}} = \frac{2}{3}\varepsilon_{O\left(NO_2 \leftrightarrow HNO_3\right)_{OH}} + \frac{1}{3}\varepsilon_{O\left(NO \leftrightarrow HNO_3\right)_{OH}}$$
$$= \frac{2}{3}\left[\frac{1000\left(^{18}\alpha_{NO_2/NO} - 1\right)\left(1 - f_{NO_2}\right)}{\left(1 - f_{NO_2}\right) + \left(^{18}\alpha_{NO_2/NO} \times f_{NO_2}\right)} + \left(\delta^{18}O\text{-}NO_x\right)\right] + \qquad (5)$$
$$\frac{1}{3}\left[\left(\delta^{18}O\text{-}H_2O\right) + 1000\left(^{18}\alpha_{OH/H_2O} - 1\right)\right]$$

301 and $\varepsilon_{O\left(NO_x \leftrightarrow pNO_3^-\right)_{H_2O}}$ can be determined as follows:

302 $$\varepsilon_{O\left(NO_x \leftrightarrow pNO_3^-\right)_{H_2O}} = \varepsilon_{O\left(NO_x \leftrightarrow HNO_3\right)_{H_2O}} = \frac{5}{6}\left(\delta^{18}O\text{-}N_2O_5\right) + \frac{1}{6}\left(\delta^{18}O\text{-}H_2O\right) \quad (6)$$

303 where $^{18}\alpha_{NO_2/NO}$ and $^{18}\alpha_{OH/H_2O}$ represent the equilibrium O isotope fractionation

304 factors between NO_2 and NO, and OH and H_2O, respectively. The range of $\delta^{18}O\text{-}H_2O$

305 can be approximated using an estimated tropospheric water vapor $\delta^{18}O$ range of -25‰-

306 0‰. The $\delta^{18}O$ values for NO_2 and N_2O_5 range from 90‰ to 122‰ (Zong et al. 2017).

307 $^{15}\alpha_{NO_2/NO}$ and $^{15}\alpha_{N_2O_5/NO_2}$, $^{18}\alpha_{NO_2/NO}$ and $^{18}\alpha_{OH/H_2O}$ in these equations, are dependent

308 on the temperature, which can be expressed as:

309 $$1000\left(^{m}\alpha_{X/Y} - 1\right) = \frac{A}{T^4} \times 10^{10} + \frac{B}{T^3} \times 10^8 + \frac{C}{T^2} \times 10^6 + \frac{D}{T} \times 10^4 \quad (7)$$

310 where A, B, C, and D are experimental constants (Table S1) over the temperature range

311 of 150-450 K (Walters and Michalski, 2015; Walters et al., 2016; Walters and Michalski,

312 2016; Zong et al., 2017).

313 Based on Equations 4-7 and measured values for $\delta^{18}O\text{-}pNO_3^-$ of ambient $PM_{2.5}$, a Monte

314 Carlo simulation was performed to generate 10000 feasible solutions. The error

315 between predicted and measured $\delta^{18}O$ was less than 0.5‰. The range (maximum and

316 minimum) of computed contribution ratios (γ) were then integrated in Equation 1 to

317 generate an estimate range for the nitrogen isotope effect ε_N (using Equations 2-3).

318 $\delta^{15}N\text{-}pNO_3^-$ values can be calculated based on ε_N and the estimated $\delta^{15}N$ range for

319 atmospheric NO_x, (see section 2.4).

2.4 Bayesian isotope mixing model

321 Isotopic mixing models allow estimating the relative contribution of multiple sources

322 (e.g., emission sources of NO_x) within a mixed pool (e.g., ambient pNO_3^-). By explicitly

323 considering the uncertainty associated with the isotopic signatures of any given source,

324 as well as isotope fractionation during the formation of various components of a mixture,

325 the application of Bayesian methods to stable isotope mixing models generates robust

326 probability estimates of source proportions, and are often more appropriate when

327 targeting natural systems than simple linear mixing models (Chang et al., 2016a). Here

328 the Bayesian model MixSIR (a stable isotope mixing model using sampling-

329 importance-resampling) was used to disentangle multiple NO_x sources by generating

330 potential solutions of source apportionment as true probability distributions, which has

331 been widely applied in a number of fields (e.g., Parnell et al., 2013; Phillips et al., 2014;

332 Zong et al., 2017). Details on the model frame and computing methods are given in SI

333 Text S1.

334 Here, coal combustion (13.72 ± 4.57‰), transportation (-3.71 ± 10.40‰), biomass

335 burning (1.04 ± 4.13‰), and biogenic emissions from soils (-33.77 ± 12.16‰) were

336 considered to be the most relevant contributors of NO_x (Table S2 and Text S2). The

337 $\delta^{15}N$ of atmospheric NO_x is unknown. However, it can be assumed that its range in the

338 atmosphere is constrained by the $\delta^{15}N$ of the NO_x sources and the $\delta^{15}N$ of $p$$NO_3^-$ after

339 equilibrium fractionation conditions have been reached. Following Zong et al. (2017),

340 $\delta^{15}N$-NO_x in the atmosphere was determined performing iterative model simulations,

341 with a simulation step of 0.01 times the equilibrium fractionation value based on the

342 $\delta^{15}N$-NO_x values of the emission sources (mean and standard deviation) and the

343 measured $\delta^{15}N$-$p$$NO_3^-$ of ambient $PM_{2.5}$ (Fig. S2).

344 **3 Results**

345 **3.1 Sanjiang in Northern China**

346 The $\delta^{15}N$-$p$$NO_3^-$ and $\delta^{18}O$-$p$$NO_3^-$ values of the eight samples collected from the

347 Sanjiang biomass burning field experiment, ranged from 9.54 to 13.77‰ (mean:

348 12.17‰) and 57.17 to 75.09‰ (mean: 63.57‰), respectively. In this study, atmospheric

349 concentrations of levoglucosan quantified from $PM_{2.5}$ samples collected near the sites

350 of biomass burning in Sanjiang vary between 4.0 and 20.5 µg m^{-3}, two to five orders of

351 magnitude higher than those measured during non-biomass burning season (Cao et al.,

352 2017; Cao et al., 2016). Levoglucosan is an anhydrosugar formed during pyrolysis of

353 cellulose at temperatures above 300 °C (Simoneit, 2002). Due to its specificity for

354 cellulose combustion, it has been widely used as a molecular tracer for biomass burning

355 (Simoneit et al., 1999; Liu et al., 2013a; Jedynska et al., 2014; Liu et al., 2014). Indeed,

356 the concentrations of levoglucosan and aerosol nitrate in Sanjiang were highly

357 correlated (R^2 = 0.64; Fig. 2a), providing compelling evidence that particulate nitrate

358 measured during our study period was predominately derived from biomass burning

359 emissions.

360 **3.2 Nanjing in Eastern China**

361 The mass concentrations $\left(mean^{max}_{min} \pm 1\sigma, n = 43\right)$ of PM$_{2.5}$ and pNO$_3^-$ measured in Nanjing

362 City were $122.1^{227.8}_{39.0} \pm 47.9$ and $17.8^{45.2}_{4.0} \pm 10.3$ µg m^{-3}, respectively. All PM$_{2.5}$

363 concentrations exceeded the Chinese Air Quality Standard for daily PM$_{2.5}$ (35 µg m^{-3}),

364 suggesting severe haze pollution during the sampling period. The corresponding δ^{15}N-

365 pNO$_3^-$ values (raw data without correction) ranged between 5.39‰ and 17.99‰,

366 indicating significant enrichment in ^{15}N relative to rural and coastal marine atmospheric

367 NO$_3^-$ sources (Table S4). This may be due to the prominent contribution of fossil fuel-

368 related NO$_x$ emissions with higher δ^{15}N values in urban areas (Elliott et al., 2007; Park

369 et al., 2018).

370 **4 Discussion**

371 **4.1 Sanjiang campaign: theoretical calculation and field validation of N isotope**

372 **fractionation during pNO$_3^-$ formation**

373 To be used as a quantitative tracer of biomass-combustion-generated aerosols,

374 levoglucosan must be conserved during its transport from its source, without partial

375 removal by reactions in the atmosphere (Hennigan et al., 2010). The mass

376 concentrations of non-sea-salt potassium (nss-K$^+$ = K$^+$ - 0.0355*Na$^+$) is considered as

377 an independent/additional indicator of biomass burning (Fig. 2b). The association of

378 elevated levels of levoglucosan with high nss-K$^+$ concentrations underscores that the

two compounds derived from the same proximate sources, and that thus aerosol levoglucosan in Sanjiang was indeed pristine and represented a reliable source indicator that is unbiased by altering processes in the atmosphere. Moreover, in our previous work (Cao et al., 2017), we observed that there was a much greater enhancement of atmospheric NO_3^- compared to SO_4^{2-} (a typical coal-related pollutant). This additionally points to biomass burning, and not coal-combustion, as the dominant pNO_3^- source in the study area, making SJ and ideal "quasi single source" environment for calibrating the N isotope effect during pNO_3^- formation.

Figure 2.

Our $\delta^{18}O$-pNO_3^- values are well within the broad range of values in previous reports (Zong et al., 2017; Geng et al., 2017; Walters and Michalski, 2016). However, as depicted in Fig. 3, the $\delta^{15}N$ values of biomass burning-emitted NO_3^- fall within the range of $\delta^{15}N$-NO_x values typically reported for emissions from coal combustion, whereas they are significantly higher than the well-established values for $\delta^{15}N$-NO_x emitted from the burning of various types of biomass (mean: 1.04 ± 4.13‰, ranging from -7 to +12‰) (Fibiger and Hastings, 2016). Turekian et al. (1998) conducted laboratory tests involving the burning of eucalyptus and African grasses, and determined that the $\delta^{15}N$ of pNO_3^- (around 23‰) was 6.6‰ higher than the $\delta^{15}N$ of the burned biomass. This implies significant N isotope partitioning during biomass burning. In the case of complete biomass combustion, by mass balance, the first gaseous products (i.e., NO_x) have the same $\delta^{15}N$ as the biomass. Hence any discrepancy between the pNO_3^- and the $\delta^{15}N$ of the biomass can be attributed to the N isotope fractionation associated with the partial conversion of gaseous NO_x to aerosol NO_3^-. Based on the computational quantum chemistry (CQC) module calculations, the N isotope fractionation ε_N $\left(mean_{min}^{max} \pm 1\sigma\right)$ determined from the Sanjiang data was

406     $10.99^{12.54}_{10.30} \pm 0.74\text{‰}$. After correcting the primary δ^{15}N-pNO$_3^-$ values under the

407   consideration of ε_N, the resulting mean δ^{15}N of $1.17^{2.98}_{-1.89} \pm 1.95\text{‰}$ is very close to the

408   N isotopic signature expected for biomass burning-emitted NO$_x$ (1.04 ± 4.13‰) (Fig.

409   3) (Fibiger and Hastings, 2016). The much higher δ^{15}N-pNO$_3^-$ values in our study

410   compared to reported δ^{15}N-NO$_x$ values for biomass burning can easily be reconciled

411   when including N isotope fractionation during the conversion of NO$_x$ to NO$_3^-$. Put

412   another way, given that Sanjiang is an environment where we can essentially exclude

413   NO$_x$ sources other than biomass burning at the time of sampling, the data nicely validate

414   our CQC module-based approach to estimate ε_N.

415

416   **Figure 3**.

417

418   **4.2 Source apportionment of NO$_x$ in an urban setting using a Bayesian isotopic**

419   **mixing model**

420   Due to its high population density and intensive industrial production, the Nanjing

421   atmosphere was expected to have high NO$_x$ concentrations derived from road traffic

422   and coal combustion (Zhao et al., 2015). However, the raw δ^{15}N-pNO$_3^-$ values (10.93 ±

423   3.32‰) fell well within the variation range of coal-emitted δ^{15}N-NO$_x$ (Fig. 3). It is

424   tempting to conclude that coal combustion is the main, or even sole, pNO$_3^-$ source

425   (given the equivalent δ^{15}N values), yet, this is very unlikely. The data rather confirm

426   that significant isotope fractionation occurred during the conversion of NO$_x$ to NO$_3^-$

427   and that, without consideration of the N isotope effect, traffic-related NO$_x$ emissions

428   will be markedly underestimated.

429   In the atmosphere, the oxygen atoms of NO$_x$ rapidly exchanged with O$_3$ in the NO/NO$_2$

430   cycle (see equations R$_1$-R$_3$) (Hastings et al., 2003), and the δ^{18}O-pNO$_3^-$ values are

431   determined by its production pathways (R$_4$-R$_7$), rather than the sources of NO$_x$

432 (Hastings et al., 2003). Thus, $\delta^{18}O$-pNO$_3^-$ can be used to gain information on the

433 pathway of conversion of NO$_x$ to nitrate in the atmosphere (Fang et al., 2011). In the

434 computational quantum chemistry module used here to calculate isotope fractionation,

435 we assumed that two-thirds of the oxygen atoms in NO$_3^-$ derive from O$_3$ and one-third

436 from •OH in the •OH generation pathway (R$_4$) (Hastings et al., 2003); correspondingly,

437 five sixths of the oxygen atoms then derived from O$_3$ and one sixth from •OH in the

438 O$_3$/H$_2$O pathway (R$_5$-R$_7$). The assumed range for $\delta^{18}O$-O$_3$ and $\delta^{18}O$-H$_2$O values were

439 90‰-122‰ and -25‰-0‰, respectively (Zong et al., 2017). The partitioning between

440 the two possible pathways was then assessed through Monte Carlo simulation (Zong et

441 al., 2017). The estimated range was rather broad, given the wide range of $\delta^{18}O$-O$_3$ and

442 $\delta^{18}O$-H$_2$O values used. Nevertheless, the theoretical calculation of the average

443 contribution ratio (γ) for nitrate formation in Nanjing via the reaction of NO$_2$ and •OH

444 is consistent with the results from simulations using the Weather Research and

445 Forecasting model coupled with Chemistry (WRF-Chem) (Fig. 4; see Text S3 for

446 details). A clear diurnal cycle of the mass concentration of nitrate formed through •OH

447 oxidation of NO$_2$ can be observed (Fig. S3), with much higher concentrations between

448 12:00 and 18:00, This indicates the importance of photochemically produced •OH

449 during daytime. Yet, throughout our sampling period in Nanjing, the average pNO$_3^-$

450 formation by the heterogeneous hydrolysis of N$_2$O$_5$ (12.6 μg m^{-3}) exceeded pNO$_3^-$

451 formation by the reaction of NO$_2$ and •OH (4.8 μg m^{-3}), even during daytime, consistent

452 with recent observations during peak pollution periods in Beijing (Wang et al., 2017).

453 Given that the production rates of N$_2$O$_5$ in the atmosphere is governed by ambient O$_3$

454 concentrations, reducing atmospheric O$_3$ levels appears to be one of the utmost

455 important measures to take for mitigating pNO$_3^-$ pollution in China's urban

456 atmospheres.

457

458 **Figure 4**.

459

In Nanjing, dependent on the time-dependent, dominant pNO$_3^-$ formation pathway, the average N isotope fractionation value calculated using the computational quantum chemistry module varied between 10.77‰ and 19.34‰ (15.33‰ on average). Using the Bayesian model MixSIR, the contribution of each source can be estimated, based on the mixed-source isotope data under the consideration of prior information on the site (see Text S1 for detailed information regarding model frame and computing method). As described above, theoretically, there are four major sources, i.e., road traffic, coal combustion, biomass burning, and biogenic soil, potentially contributing to ambient NO$_x$. As a start, we tentatively integrated all four sources into MixSIR (data not shown). The relative contribution of biomass burning to the ambient NO$_x$ (median value) ranged from 28% to 70% (average 42%), representing the most important source. The primary reason for such apparently high contribution by biomass burning is that the corrected δ^{15}N-pNO$_3^-$ values of $-4.29^{0.42}_{-10.32} \pm 3.66$‰ are relatively close to the N isotopic signature of biomass burning-emitted NO$_x$ (1.04 ± 4.13‰) compared to the other possible sources. Based on δ^{15}N alone, the isotope approach can be ambiguous if there are more than two sources. The N isotope signature of NO$_x$ from biomass burning falls right in between the spectrum of plausible values, with highest δ^{15}N for emissions from coal combustion on the one end, and much lower values for automotive and soil emissions on the other, and will be similar to a mixed signature from coal combustion and NO$_x$ emissions from traffic.

We can make several evidence-based pre-assumption to better constrain the emission sources in the mixing model analysis: (1) sampling at a typical urban site in a major industrial city in China, we can assume that the sources of road traffic and coal combustion are dominant, while the contribution of biogenic soil to ambient NO$_x$ should have minimal impact, or can be largely neglected (Zhao et al., 2015); (2) there is no crop harvest activity in Eastern China during the winter season. Furthermore, deforestation and combustion of fuelwood has been discontinued in China's major cities (Chang et al., 2016a). Therefore, the contribution of biomass burning-emitted NO$_x$ during the sampling period should also be minor. Indeed, Fig. S4 shows that the

489   mass concentration of biomass burning-related pNO$_3^-$ is not correlated with the fraction

490   of levoglucosan that contributes to OC, confirming a weak impact of biomass burning

491   on the variation of pNO$_3^-$ concentration during our study period.

492   In a second, alternative, and more realistic scenario, we excluded biomass burning and

493   soil as potential source of NO$_x$ in MixSIR (see above). As illustrated in Fig. 5a,

494   assuming that NO$_x$ emissions in urban Nanjing during our study period originated

495   solely from road traffic and coal combustion, their relative contribution to the mass

496   concentration of pNO$_3^-$ is 12.5 ± 9.1 μg m^{-3} (or 68 ± 11%) and 4.9 ± 2.5 μg m^{-3} (or 32

497   ± 11%), respectively. These numbers agree well with a city-scale NO$_x$ emission

498   inventory established for Nanjing recently (Zhao et al., 2015). Nevertheless, on a

499   nation-wide level, relatively large uncertainties with regards to the overall fossil fuel

500   consumption and fuel types propagate into large uncertainties of NO$_x$ concentration

501   estimates and predictions of longer-term emission trends (Li et al., 2017). Current

502   emission-inventory estimates (Jaegle et al., 2005; Zhang et al., 2012; Liu et al., 2015;

503   Zhao et al., 2013) suggest that in 2010 NO$_x$ emissions from coal-fired power plants in

504   China were about 30% higher than those from transportation. However, our isotope-

505   based source apportionment of NO$_x$ clearly shows that in 2014 the contribution from

506   road traffic to NO$_x$ emissions, at least in Nanjing (a city that can be considered

507   representative for most densely populated areas in China) is twice that of coal

508   combustion. In fact, due to changing economic activities, emission sources of air

509   pollutants in China are changing rapidly. For example, over the past several years,

510   China has implemented an extended portfolio of plans to phase out its old-fashioned

511   and small power plants, and to raise the standards for reducing industrial pollutant

512   emissions (Chang, 2012). On the other hand, China continuously experienced double-

513   digit annual growth in terms of auto sales during the 2000s, and in 2009 it became the

514   world's largest automobile market (Liu et al., 2013b; Chang et al., 2017; Chang et al.,

515   2016b). Recent satellite-based studies successfully analyzed the NO$_x$ vertical column

516   concentration ratios for megacities in Eastern China and highlighted the importance of

517   transportation-related NOx emissions (Reuter et al., 2014; Gu et al., 2014; Duncan et

al., 2016; Jin et al., 2017). Moreover, long-term measurements of the ratio of NO_3^- versus non-sea-salt SO_4^{2-} in precipitation and aerosol jointly revealed a continuously increasing trend in Eastern China throughout the latest decade, suggesting decreasing emissions from coal combustion (Liu et al., 2013b; Itahashi et al., 2017). Both coal combustion- and road traffic-related pNO_3^- concentrations are highly correlated with their corresponding tracers (i.e., SO_2 and CO, respectively), confirming the validity of our MixSIR modelling results. With justified confidence in our Bayesian isotopic model results, we conclude that previous estimates of NO_x emissions from automotive/transportation sources in China based on bottom-up emission inventories may be too low.

Figure 5.

3.3 Previous $\delta^{15}N$-NO_3^- based estimates on NO_x sources

Stable nitrogen isotope ratios of nitrate have been used to identify nitrogen sources in various environments in China, often without large differences in $\delta^{15}N$ between rainwater and aerosol NO_3^- (Kojima et al., 2011). In previous work, no consideration was given to potential N isotope fractionation during atmospheric pNO_3^- formation. Here, we reevaluated 700 data points of $\delta^{15}N$-NO_3^- in aerosol (-0.77 ± 4.52‰, n = 308) and rainwater (3.79 ± 6.14‰, n = 392) from 13 sites that are located in the area of mainland China and the Yellow and East and South China Seas (Fig. 1), extracted from the literature (see SI Table S4 for details). To verify the potentially biasing effects of neglecting N isotope fractionation (i.e. testing the sensitivity of ambient NO_x source contribution estimates to the effect of N isotope fractionation), the Bayesian isotopic mixing model was applied a) to the original NO_3^- isotope data set and b) to the corrected nitrate isotope data set, accounting for the N isotope fractionation during NO_x transformation. All 13 sampling sites are located in non-urban areas; therefore, apart

545 from coal combustion and on-road traffic, the contributions of biomass burning and

546 biogenic soil to nitrate needs to be taken into account.

547 Although most of the sites are located in rural and coastal environments, using the

548 original data set without the consideration of N isotope fractionation in the Bayesian

549 isotopic mixing model, fossil fuel-related NO_x emissions (coal combustion and on-road

550 traffic) appear as the largest contributor at all the sites (data are not shown). This is

551 particularly true for coal combustion: Everywhere, except for the sites of Dongshan

552 Islands and Mt. Lumin, NO_x emissions seem to be dominated by coal combustion. Very

553 high contribution from coal combustion (on the order of 40-60%) particularly in

554 Northern China may be plausible, and can be attributed to a much larger consumption

555 of coal. Yet, rather unlikely, the highest estimated contribution of coal combustion (83%)

556 was calculated for Beihuang Island (a full-year sampling at a costal island that is 65 km

557 north of Shandong Peninsula and 185 km east of the Beijing-Tianjin-Hebei region) and

558 not for mainland China. While Beihuang may be an extreme example, we argue that,

559 collectively, the contribution of coal combustion to ambient NO_x in China as calculated

560 on the basis of isotopic analyses in previous studies without the consideration of N

561 isotope fractionation represent overestimates.

562 As a first step towards a more realistic assessment of the actual partitioning of NO_x

563 sources in China in general (and coal combustion-emitted NO_x in particular), it is

564 imperative to determine the location-specific values for ε_N. Unfortunately, without

565 $\delta^{18}O\text{-}NO_3^-$ data in hand, as well as data on meteorological parameters that correspond

566 to the 700 $\delta^{15}N\text{-}NO_3^-$ values used in our meta-analysis, it is not possible to estimate the

567 ε_N values through the above-mentioned CQC module. As a viable alternative, we

568 adopted the approximate values for ε_N as estimated in Sanjiang (10.99‰) and Nanjing

569 (15.33 ± 4.90‰). As indicated in Fig. 6, the estimates on the source partitioning is

570 sensitive to the choice of ε_N. Whereas with increasing ε_N, estimates on the relative

571 contribution of on-road traffic and biomass burning remained relatively stable;

572 estimates for coal combustion and biogenic soil changed significantly, in opposite

573   directions. More precisely, depending on ε_N, the average estimate of the fractional

574   contribution of coal combustion decreased drastically from 43% ($\varepsilon_N = 0‰$) to 5% (ε_N

575   $= 20‰$) (Fig. 6), while the contribution from biogenic soil to NO_x emissions increased

576   in a complementary way. Given the lack of better constraints on ε_N for the 13 sampling

577   sites, it cannot be our goal here to provide a robust revised estimate on the partitioning

578   of NO_x sources throughout China and its neighboring areas. But we have very good

579   reasons to assume that disregard of N isotope fractionation during pNO_3^- formation in

580   previous isotope-based source apportionment studies has likely led to overestimates of

581   the relative contribution of coal combustion to total NO_x emissions in China. For what

582   we would consider the most conservative estimate, i.e. lowest calculated value for the

583   N isotope fractionation during the transformation of NO_x to pNO_3^- ($\varepsilon_N = 5‰$), the

584   approximate contribution from coal combustion to the NO_x pool would be 28%, more

585   than 30% less than N isotope mixing model-based estimates would yield without

586   consideration of the N isotope fractionation (i.e., $\varepsilon N = 0‰$) (Fig. 6).

587

588   **Figure 6.**

589

590

591   **4 Conclusion and outlook**

592   Consistent with theoretical predictions, $\delta^{15}N\text{-}pNO_3^-$ data from a field experiment where

593   atmospheric pNO_3^- formation could be attributed reliably to NO_x from biomass burning

594   only, revealed that the conversion of NO_x to pNO_3^- is associated with a significant net

595   N isotope effect (ε_N). It is imperative that future studies, making use of isotope mixing

596   models to gain conclusive constraints on the source partitioning of atmospheric NO_x,

597   will consider this N isotope fractionation. The latter will change with time and space,

598   depending on the distribution of ozone and OH radicals in the atmosphere and the

predominant NO_x chemistry. The O-isotope signatures of pNO_3^- is mostly chemistry- (and not source) driven (modulated by O-isotope exchange reactions in the atmosphere), and thus, O isotope measurements do not allow addressing the ambiguities with regards to the NO_x source that may remain when just looking at $\delta^{15}N$ values alone. However, $\delta^{18}O$ in pNO_3^- will help assessing the relative importance of the dominant pNO_3^- formation pathway. Simultaneous $\delta^{15}N$ and $\delta^{18}O$ measurements of atmospheric nitrate thus allow reliable information on ε_N, and in turn on the relative importance of single NO_x sources. For example, for Nanjing, which can be considered representative for other large cities in China, dual-isotopic and chemical-tracer evidence suggest that on-road traffic and coal-fired power plants, rather than biomass burning, are the predominant sources during high-haze pollution periods. Given that the increasing frequency of nitrate-driven haze episodes in China, our findings are critically important in terms of guiding the use of stable nitrate isotope measurements to evaluate the relative importance of single NO_x sources on regional scales, and for adapting suitable mitigation measures. Future assessments of NO_x emissions in China (and elsewhere) should involve simultaneous $\delta^{15}N$ and $\delta^{18}O$ measurements of atmospheric nitrate and NO_x at high spatiotemporal resolution, allowing us to more quantitatively reevaluate former N-isotope based NO_x source partitioning estimates.

Competing interests

The authors declare that they have no competing interests.

Data availability

Data are available from the corresponding author on request. We prefer not to publish the software of calculating the nitrogen isotope fractionation factor and estimating nitrate source attribution at the present stage in order to avoid compromising the future of ongoing software registration. Readers can download the software through the website atmosgeochem.com after the finish of software registration.

Acknowledgement

This study was supported by the National Key Research and Development Program of

China (2017YFC0210101), the National Natural Science Foundation of China (Grant nos. 91644103, 41705100, and 41575129), the Provincial Natural Science Foundation of Jiangsu (BK20170946), the University Science Research Project of Jiangsu Province (17KJB170011), the International Joint Laboratory on Climate and Environment Change (ILCEC) and the Collaborative Innovation Center on Forecast and Evaluation of Meteorological Disasters (CIC-FEMD) through NUIST, and through University Basel Research funds.

Reference

Alexander, B., Hastings, M. G., Allman, D. J., Dachs, J., Thornton, J. A., and Kunasek, S. A.: Quantifying atmospheric nitrate formation pathways based on a global model of the oxygen isotopic composition (Δ^{17}O) of atmospheric nitrate, Atmos. Chem. Phys., 9, 5043-5056, doi: 10.5194/acp-9-5043-2009, 2009.

Altieri, K. E., Hastings, M. G., Gobel, A. R., Peters, A. J., and Sigman, D. M.: Isotopic composition of rainwater nitrate at Bermuda: the influence of air mass source and chemistry in the marine boundary layer, J. Geophys. Res., 118, 11, 304-311, 316, doi: 10.1002/jgrd.50829, 2013.

Anenberg, S. C., Miller, J., Minjares, R., Du, L., Henze, D. K., Lacey, F., Malley, C. S., Emberson, L., Franco, V., Klimont, Z., and Heyes, C.: Impacts and mitigation of excess diesel-related NO_x emissions in 11 major vehicle markets, Nature, 545, 467-471, doi: 10.1038/nature22086, 2017.

Böhlke, J. K., Mroczkowski, S. J., and Coplen, T. B.: Oxygen isotopes in nitrate: new reference materials for ^{18}O:^{17}O:^{16}O measurements and observations on nitrate-water equilibration, Rapid Commun. Mass Sp., 17, 1835-1846, doi: 10.1002/rcm.1123, 2003.

Cao, F., Zhang, S. C., Kawamura, K., and Zhang, Y. L.: Inorganic markers, carbonaceous components and stable carbon isotope from biomass burning aerosols in Northeast China, Sci. Total Environ., 572, 1244-1251, doi: 10.1016/j.scitotenv.2015.09.099, 2016.

Cao, F., Zhang, S. C., Kawamura, K., Liu, X., Yang, C., Xu, Z., Fan, M., Zhang, W., Bao, M., Chang, Y., Song, W., Liu, S., Lee, X., Li, J., Zhang, G., and Zhang, Y. L.: Chemical characteristics of dicarboxylic acids and related organic compounds in $PM_{2.5}$ during biomass-burning and non-biomass-burning seasons at a rural site of Northeast China, Environ. Pollut., 231, 654-662, doi: 10.1016/j.envpol.2017.08.045, 2017.

Casciotti, K. L., Sigman, D. M., Hastings, M. G., Böhlke, J. K., and Hilkert, A.: Measurement of the oxygen isotopic composition of nitrate in seawater and freshwater using the denitrifier method, Anal. Chem., 74, 4905-4912, doi: 10.1021/ac020113w, 2002.

Chang, Y. H.: China needs a tighter $PM_{2.5}$ limit and a change in priorities, Environ. Sci.

Technol., 46, 7069-7070, doi: 10.1021/es3022705, 2012.

Chang, Y. H., Deng, C., Cao, F., Cao, C., Zou, Z., Liu, S., Lee, X., Li, J., Zhang, G., and Zhang, Y.: Assessment of carbonaceous aerosols in Shanghai, China - Part 1: long-term evolution, seasonal variations, and meteorological effects, Atmos. Chem. Phys., 17, 9945-9964, doi: 10.5194/acp-17-9945-2017, 2017.

Chang, Y. H., Liu, X., Deng, C., Dore, A. J., and Zhuang, G.: Source apportionment of atmospheric ammonia before, during, and after the 2014 APEC summit in Beijing using stable nitrogen isotope signatures, Atmos. Chem. Phys., 16, 11635-11647, doi: 10.5194/acp-16-11635-2016, 2016a.

Chang, Y. H., Zou, Z., Deng, C., Huang, K., Collett, J. L., Lin, J., and Zhuang, G.: The importance of vehicle emissions as a source of atmospheric ammonia in the megacity of Shanghai, Atmos. Chem. Phys., 16, 3577-3594, doi: 10.5194/acp-16-3577-2016, 2016b.

Duncan, B. N., Lamsal, L. N., Thompson, A. M., Yoshida, Y., Lu, Z., Streets, D. G., Hurwitz, M. M., and Pickering, K. E.: A space-based, high-resolution view of notable changes in urban NO_x pollution around the world (2005-2014), J. Geophys. Res., 121, 976-996, doi: 10.1002/2015JD024121, 2016.

Elliott, E., Kendall, C., Wankel, S. D., Burns, D., Boyer, E., Harlin, K., Bain, D., and Butler, T.: Nitrogen isotopes as indicators of NO_x source contributions to atmospheric nitrate deposition across the midwestern and northeastern United States, Environ. Sci. Technol., 41, 7661-7667, doi: 10.1021/es070898t, 2007.

Elliott, E. M., Kendall, C., Boyer, E. W., Burns, D. A., Lear, G. G., Golden, H. E., Harlin, K., Bytnerowicz, A., Butler, T. J., and Glatz, R.: Dual nitrate isotopes in dry deposition: Utility for partitioning NO_x source contributions to landscape nitrogen deposition, J. Geophys. Res., 114, doi: 10.1029/2008jg000889, 2009.

Fang, Y. T., Koba, K., Wang, X. M., Wen, D. Z., Li, J., Takebayashi, Y., Liu, X. Y., and Yoh, M.: Anthropogenic imprints on nitrogen and oxygen isotopic composition of precipitation nitrate in a nitrogen-polluted city in southern China, Atmos. Chem. Phys., 11, 1313-1325, doi: 10.5194/acp-11-1313-2011, 2011.

Felix, J. D., and Elliott, E. M.: Isotopic composition of passively collected nitrogen dioxide emissions: Vehicle, soil and livestock source signatures, Atmos. Environ., 92, 359-366, doi: 10.1016/j.atmosenv.2014.04.005, 2014.

Felix, J. D., Elliott, E. M., Gish, T. J., McConnell, L. L., and Shaw, S. L.: Characterizing the isotopic composition of atmospheric ammonia emission sources using passive samplers and a combined oxidation-bacterial denitrifier approach, Rapid Comm. Mass spec., 27, 2239-2246, doi: 10.1002/rcm.6679, 2013.

Felix, J. D., Elliott, E. M., and Shaw, S. L.: Nitrogen isotopic composition of coal-fired power plant NO_x: Influence of emission controls and implications for global emission inventories, Environ. Sci. Technol., 46, 3528-3535, doi: 10.1021/es203355v, 2012.

Fibiger, D. L., and Hastings, M. G.: First measurements of the nitrogen isotopic composition of NO_x from biomass burning, Environ. Sci. Technol., 50, 11569-11574, doi: 10.1021/acs.est.6b03510, 2016.

Freyer, H. D.: Seasonal trends of NH_4^+ and NO_3^- nitrogen isotope composition in rain collected at Jülich, Germany, Tellus, 30, 83-92, 1978.

Freyer, H. D.: Seasonal variation of ^{15}N/^{14}N ratios in atmospheric nitrate species, Tellus, 43, 30-44, doi: 10.3402/tellusb.v43i1.15244, 2017.

Freyer, H. D., Kley, D., Volz-Thomas, A., and Kobel, K.: On the interaction of isotopic exchange processes with photochemical reactions in atmospheric oxides of nitrogen, J. Geophys. Res., 98, 14791-14796, doi: 10.1029/93JD00874, 1993.

Fu, X., Wang, S., Zhao, B., Xing, J., Cheng, Z., Liu, H., and Hao, J.: Emission inventory of primary pollutants and chemical speciation in 2010 for the Yangtze River Delta region, China, Atmos. Environ., 70, 39-50, doi: 10.1016/j.atmosenv.2012.12.034, 2013.

Galloway, J. N., Aber, J. D., Erisman, J. W., Seitzinger, S. P., Howarth, R. W., Cowling, E. B., and Cosby, B. J.: The nitrogen cascade, Biosci., 53, 341-356, doi: 10.1641/0006-3568(2003)053[0341:Tnc]2.0.Co;2, 2003.

Geng, L., Murray, L. T., Mickley, L. J., Lin, P., Fu, Q., Schauer, A. J., and Alexander, B.: Isotopic evidence of multiple controls on atmospheric oxidants over climate transitions, Nature, 546, 133-136, doi: 10.1038/nature22340, 2017.

Gobel, A. R., Altieri, K. E., Peters, A. J., Hastings, M. G., and Sigman, D. M.: Insights into anthropogenic nitrogen deposition to the North Atlantic investigated using the isotopic composition of aerosol and rainwater nitrate, Geophys. Res. Lett., 40, 5977-5982, doi: 10.1002/2013GL058167, 2013.

Gu, D., Wang, Y., Smeltzer, C., and Boersma, K. F.: Anthropogenic emissions of NO_x over China: Reconciling the difference of inverse modeling results using GOME-2 and OMI measurements, J. Geophys. Res., 119, 7732-7740, doi: 10.1002/2014JD021644, 2014.

Hastings, M. G., Sigman, D. M., and Lipschultz, F.: Isotopic evidence for source changes of nitrate in rain at Bermuda, J. Geophys. Res., 108, doi: 10.1029/2003JD003789, 2003.

Heaton, T. H. E.: ^{15}N/^{14}N ratios of NO_x from vehicle engines and coal-fired power stations, Tellus, 42, 304-307, doi: 10.1034/j.1600-0889.1990.00007.x-i1, 1990.

Hennigan, C. J., Sullivan, A. P., Collett, J. L., and Robinson, A. L.: Levoglucosan stability in biomass burning particles exposed to hydroxyl radicals, Geophys. Res. Lett., 37, doi: 10.1029/2010GL043088, 2010.

Hoering, T.: The isotopic composition of the ammonia and the nitrate ion in rain, Geochim. Cosmochim. Ac., 12, 97-102, doi: 10.1016/0016-7037(57)90021-2, 1957.

Itahashi, S., Yumimoto, K., Uno, I., Hayami, H., Fujita, S. I., Pan, Y., and Wang, Y.: A 15-year record (2001-2015) of the ratio of nitrate to non-seasalt sulfate in precipitation over East Asia, Atmos. Chem. Phys. Discuss., 2017, 1-30, doi: 10.5194/acp-2017-848, 2017.

Jaegle, L., Steinberger, L., Martin, R. V., and Chance, K.: Global partitioning of NO_x sources using satellite observations: Relative roles of fossil fuel combustion, biomass burning and soil emissions, Faraday Discus., 130, 407-423, doi: 10.1039/B502128F, 2005.

Jedynska, A., Hoek, G., Wang, M., Eeftens, M., Cyrys, J., Beelen, R., Cirach, M., De Nazelle, A., Nystad, W., Makarem Akhlaghi, H., Meliefste, K., Nieuwenhuijsen, M., de Hoogh, K., Brunekreef, B., and Kooter, I. M.: Spatial variations and development

of land use regression models of levoglucosan in four European study areas, Atmos. Chem. Phys. Discuss., 2014, 13491-13527, doi: 10.5194/acpd-14-13491-2014, 2014.

Ji, S., Cherry, C. R., Zhou, W., Sawhney, R., Wu, Y., Cai, S., Wang, S., and Marshall, J. D.: Environmental justice aspects of exposure to $PM_{2.5}$ emissions from electric vehicle use in China, Environ. Sci. Technol., 49, 13912-13920, doi: 10.1021/acs.est.5b04927, 2015.

Jin, X., Fiore, A. M., Murray, L. T., Valin, L. C., Lamsal, L. N., Duncan, B., Folkert Boersma, K., De Smedt, I., Abad, G. G., Chance, K., and Tonnesen, G. S.: Evaluating a space-based indicator of surface ozone-NO_x-VOC sensitivity over midlatitude source regions and application to decadal trends, J. Geophys. Res., 122, 439-461, doi: 10.1002/2017JD026720, 2017.

Kaiser, J. C., Riemer, N., and Knopf, D. A.: Detailed heterogeneous oxidation of soot surfaces in a particle-resolved aerosol model, Atmos. Chem. Phys., 11, 4505-4520, doi: 10.5194/acp-11-4505-2011, 2011.

Kendall, C., Elliott, E. M., and Wankel, S. D.: Stable isotopes in ecology and environmental science, chapter 12, 2nd Edition, Blackwell, Oxford, 2007.

Knopf, D. A., Forrester, S. M., and Slade, J. H.: Heterogeneous oxidation kinetics of organic biomass burning aerosol surrogates by O_3, NO_2, N_2O_5, and NO_3, Phys. Chem. Chem. Phys., 13, 21050-21062, doi: 10.1039/C1CP22478F, 2011.

Knopf, D. A., Mak, J., Gross, S., and Bertram, A. K.: Does atmospheric processing of saturated hydrocarbon surfaces by NO_3 lead to volatilization?, Geophys. Res. Lett., 33, doi:10.1029/2006GL026884, 2006.

Kojima, K., Murakami, M., Yoshimizu, C., Tayasu, I., Nagata, T., and Furumai, H.: Evaluation of surface runoff and road dust as sources of nitrogen using nitrate isotopic composition, Chemosphere, 84, 1716-1722, doi: 10.1016/j.chemosphere.2011.04.071, 2011.

Lamsal, L. N., Martin, R. V., Padmanabhan, A., van Donkelaar, A., Zhang, Q., Sioris, C. E., Chance, K., Kurosu, T. P., and Newchurch, M. J.: Application of satellite observations for timely updates to global anthropogenic NO_x emission inventories, Geophy. Res. Lett., 38, doi: 10.1029/2010GL046476, 2011.

Leighton, P.: Photochemistry of Air Pollution, Academic, New York, 1961.

Levy, H., Moxim, W. J., and Kasibhatla, P. S.: A global three-dimensional time-dependent lightning source of tropospheric NO_x, J. Geophys. Res., 101, 22911-22922, doi: 10.1029/96JD02341, 1996.

Li, D., and Wang, X.: Nitrogen isotopic signature of soil-released nitric oxide (NO) after fertilizer application, Atmos. Environ., 42, 4747-4754, doi: 10.1016/j.atmosenv.2008.01.042, 2008.

Li, M., Zhang, Q., Kurokawa, J. I., Woo, J. H., He, K., Lu, Z., Ohara, T., Song, Y., Streets, D. G., Carmichael, G. R., Cheng, Y., Hong, C., Huo, H., Jiang, X., Kang, S., Liu, F., Su, H., and Zheng, B.: MIX: a mosaic Asian anthropogenic emission inventory under the international collaboration framework of the MICS-Asia and HTAP, Atmos. Chem. Phys., 17, 935-963, doi: 10.5194/acp-17-935-2017, 2017.

Ling, T. Y., and Chan, C. K.: Formation and transformation of metastable double salts from the crystallization of mixed ammonium nitrate and ammonium sulfate particles,

798   Environ. Sci. Technol., 41, 8077-8083, doi: 10.1021/es071419t, 2007.

799   Liu, D., Li, J., Zhang, Y., Xu, Y., Liu, X., Ding, P., Shen, C., Chen, Y., Tian, C., and
800   Zhang, G.: The use of levoglucosan and radiocarbon for source apportionment of
801    $PM_{2.5}$ carbonaceous aerosols at a background site in East China, Environ. Sci.
802   Technol., 47, 10454-10461, doi: 10.1021/es401250k, 2013a.

803   Liu, F., Zhang, Q., Tong, D., Zheng, B., Li, M., Huo, H., and He, K. B.: High-resolution
804   inventory of technologies, activities, and emissions of coal-fired power plants in
805   China from 1990 to 2010, Atmos. Chem. Phys., 15, 13299-13317, doi: 10.5194/acp-
806   15-13299-2015, 2015.

807   Liu, J., Li, J., Zhang, Y., Liu, D., Ding, P., Shen, C., Shen, K., He, Q., Ding, X., Wang,
808   X., Chen, D., Szidat, S., and Zhang, G.: Source apportionment using radiocarbon and
809   organic tracers for $PM_{2.5}$ carbonaceous aerosols in Guangzhou, South China:
810   contrasting local- and regional-scale haze events, Environ. Sci. Technol., 48, 12002-
811   12011, doi: 10.1021/es503102w, 2014.

812   Liu, X., Zhang, Y., Han, W., Tang, A., Shen, J., Cui, Z., Vitousek, P., Erisman, J. W.,
813   Goulding, K., Christie, P., Fangmeier, A., and Zhang, F.: Enhanced nitrogen
814   deposition over China, Nature, 494, 459-463, doi: 10.1038/nature11917, 2013b.

815   Lu, Z., Streets, D. G., de Foy, B., Lamsal, L. N., Duncan, B. N., and Xing, J.: Emissions
816   of nitrogen oxides from US urban areas: estimation from Ozone Monitoring
817   Instrument retrievals for 2005-2014, Atmos. Chem. Phys., 15, 10367-10383, doi:
818   10.5194/acp-15-10367-2015, 2015.

819   Michalski, G., Scott, Z., Kabiling, M., and Thiemens, M. H.: First measurements and
820   modeling of $\Delta^{17}O$ in atmospheric nitrate, Geophys. Res. Lett., 30, 1870-1872, doi:
821   10.1029/2003gl017015, 2003.

822   Miyazaki, K., Eskes, H., Sudo, K., Boersma, K. F., Bowman, K., and Kanaya, Y.:
823   Decadal changes in global surface NO_x emissions from multi-constituent satellite
824   data assimilation, Atmos. Chem. Phys., 17, 807-837, doi: 10.5194/acp-17-807-2017,
825   2017.

826   Morin, S., Savarino, J., Frey, M. M., Yan, N., Bekki, S., Bottenheim, J. W., and Martins,
827   J. M.: Tracing the origin and fate of NO_x in the Arctic atmosphere using stable
828   isotopes in nitrate, Science, 322, 730-732, doi: 10.1126/science.1161910, 2008.

829   Morino, Y., Kondo, Y., Takegawa, N., Miyazaki, Y., Kita, K., Komazaki, Y., Fukuda,
830   M., Miyakawa, T., Moteki, N., and Worsnop, D. R.: Partitioning of HNO_3 and
831   particulate nitrate over Tokyo: Effect of vertical mixing, J. Geophys. Res., 111, doi:
832   10.1029/2005JD006887, 2006.

833   Park, Y. M., Park, K. S., Kim, H., Yu, S. M., Noh, S., Kim, M. S., Kim, J. Y., Ahn, J. Y.,
834   Lee, M. D., Seok, K. S., and Kim, Y. H.: Characterizing isotopic compositions of TC-
835   C, NO_3^--N, and NH_4^+-N in $PM_{2.5}$ in South Korea: Impact of China's winter heating,
836   Environ. Pollut., 233, 735-744, doi: 10.1016/j.envpol.2017.10.072, 2018.

837   Parnell, A. C., Phillips, D. L., Bearhop, S., Semmens, B. X., Ward, E. J., Moore, J. W.,
838   Jackson, A. L., Grey, J., Kelly, D. J., and Inger, R.: Bayesian stable isotope mixing
839   models, Environmetrics, 24, 387-399, doi: 10.1002/env.2221, 2013.

840   Phillips, D. L., Inger, R., Bearhop, S., Jackson, A. L., Moore, J. W., Parnell, A. C.,
841   Semmens, B. X., and Ward, E. J.: Best practices for use of stable isotope mixing

842   models in food-web studies, Can. J. Zool., 92, 823-835, doi: 10.1139/cjz-2014-0127,
843   2014.

844   Price, C., Penner, J., and Prather, M.: NO_x from lightning: 1. Global distribution based
845   on lightning physics, J. Geophys. Res., 102, 5929-5941, doi: 10.1029/96JD03504,
846   1997.

847   Reuter, M., Buchwitz, M., Hilboll, A., Richter, A., Schneising, O., Hilker, M., Heymann,
848   J., Bovensmann, H., and Burrows, J. P.: Decreasing emissions of NOx relative to CO_2
849   in East Asia inferred from satellite observations, Nat. Geosci., 7, 792-795, doi:
850   10.1038/ngeo2257, 2014.

851   Richter, A., Burrows, J. P., Nüß, H., Granier, C., and Niemeier, U.: Increase in
852   tropospheric nitrogen dioxide over China observed from space, Nature, 437, 129, doi:
853   10.1038/nature04092, 2005.

854   Savarino, J., Kaiser, J., Morin, S., Sigman, D., and Thiemens, M.: Nitrogen and oxygen
855   isotopic constraints on the origin of atmospheric nitrate in coastal Antarctica, Atmos.
856   Chem. Phys., 7, 1925-1945, doi: 10.5194/acp-7-1925-2007, 2007.

857   Seinfeld, J. H., and Pandis, S. N.: Atmospheric chemistry and physics: From air
858   pollution to climate change, John Wiley & Sons, 2012.

859   Shiraiwa, M., Pöschl, U., and Knopf, D. A.: Multiphase chemical kinetics of NO_3
860   radicals reacting with organic aerosol components from biomass burning, Environ.
861   Sci. Technol., 46, 6630-6636, doi: 10.1021/es300677a, 2012.

862   Sigman, D. M., Casciotti, K. L., Andreani, M., Barford, C., Galanter, M., and Böhlke,
863   J. K.: A bacterial method for the nitrogen isotopic analysis of nitrate in seawater and
864   freshwater, Anal. Chem., 73, 4145-4153, doi: 10.1021/ac010088e, 2001.

865   Simoneit, B. R. T., Schauer, J. J., Nolte, C. G., Oros, D. R., Elias, V. O., Fraser, M. P.,
866   Rogge, W. F., and Cass, G. R.: Levoglucosan, a tracer for cellulose in biomass
867   burning and atmospheric particles, Atmos. Environ., 33, 173-182, Anal. Chem., doi:
868   10.1016/S1352-2310(98)00145-9, 1999.

869   Simoneit, B. R. T.: Biomass burning - a review of organic tracers for smoke from
870   incomplete combustion, Appl. Geochem., 17, 129-162, Anal. Chem., doi:
871   10.1016/S0883-2927(01)00061-0, 2002.

872   Smith, M. L., Bertram, A. K., and Martin, S. T.: Deliquescence, efflorescence, and
873   phase miscibility of mixed particles of ammonium sulfate and isoprene-derived
874   secondary organic material, Atmos. Chem. Phys., 12, 9613-9628, doi: 10.5194/acp-
875   12-9613-2012, 2012.

876   Solomon, S., Qin, D., Manning, M., Chen, Z., Marquis, M., Averyt, K. B., Tignor, M.,
877   and Miller, H. L.: Climate change 2007: The physical science basis: contribution of
878   Working Group I to the Fourth Assessment Report of the Intergovernmental Panel on
879   Climate Change, Cambridge University Press, New York, 2007.

880   Thiemens, M. H., and Heidenreich, J. E.: The mass-independent fractionation of oxygen:
881   a novel isotope effect and its possible cosmochemical implications, Science, 219,
882   1073-1075, doi: 10.1126/science.219.4588.1073, 1983.

883   Thiemens, M. H.: Mass-independent isotope effects in planetary atmospheres and the
884   early solar system, Science, 283, 341-345, doi: 10.1126/science.283.5400.341, 1999.

885   Turekian, V. C., Macko, S., Ballentine, D., Swap, R. J., and Garstang, M.: Causes of

bulk carbon and nitrogen isotope fractionations in the products of vegetation burns: laboratory studies, Chem. Geol., 152, 181-192, doi: 10.1016/S0009-2541(98)00105-3, 1998.

Walters, W. W., Goodwin, S. R., and Michalski, G.: Nitrogen stable isotope composition (δ^{15}N) of vehicle-emitted NO_x, Environ. Sci. Technol., 49, 2278-2285, doi: 10.1021/es505580v, 2015.

Walters, W. W., and Michalski, G.: Theoretical calculation of nitrogen isotope equilibrium exchange fractionation factors for various NO_y molecules, Geochim. Cosmochim. Ac., 164, 284-297, doi: 10.1016/j.gca.2015.05.029, 2015.

Walters, W. W., and Michalski, G.: Theoretical calculation of oxygen equilibrium isotope fractionation factors involving various NO_y molecules, OH, and H_2O and its implications for isotope variations in atmospheric nitrate, Geochim. Cosmochim. Ac., 191, 89-101, doi: 10.1016/j.gca.2016.06.039, 2016.

Walters, W. W., Simonini, D. S., and Michalski, G.: Nitrogen isotope exchange between NO and NO_2 and its implications for δ^{15}N variations in tropospheric NO_x and atmospheric nitrate, Geophys. Res. Lett., 43, 440-448, doi: 10.1002/2015gl066438, 2016.

Wang, H., Lu, K., Chen, X., Zhu, Q., Chen, Q., Guo, S., Jiang, M., Li, X., Shang, D., Tan, Z., Wu, Y., Wu, Z., Zou, Q., Zheng, Y., Zeng, L., Zhu, T., Hu, M., and Zhang, Y.: High N_2O_5 concentrations observed in urban Beijing: Implications of a large nitrate formation pathway, Environ. Sci. Technol. Lett., 4, 416-420, doi: 10.1021/acs.estlett.7b00341, 2017.

Wankel, S. D., Chen, Y., Kendall, C., Post, A. F., and Paytan, A.: Sources of aerosol nitrate to the Gulf of Aqaba: Evidence from δ^{15}N and δ^{18}O of nitrate and trace metal chemistry, Mar. Chem., 120, 90-99, doi: 10.1016/j.marchem.2009.01.013, 2010.

Wojtal, P. K., Miller, D. J., O'Conner, M., Clark, S. C., and Hastings, M. G.: Automated, high-resolution mobile collection system for the nitrogen isotopic analysis of NO_x, J. Vis. Exp., 118, e54962, doi: 10.3791/54962, 2016.

Yienger, J. J., and Levy, H.: Empirical model of global soil-biogenic NO_x emissions, J. Geophys. Res., 100, 11447-11464, doi: 10.1029/95JD00370, 1995.

Zhang, Q., Geng, G., Wang, S., Richter, A., and He, K.: Satellite remote sensing of changes in NO_x emissions over China during 1996-2010, Chinese Sci. Bull., 57, 2857-2864, doi: 10.1007/s11434-012-5015-4, 2012.

Zhang, R., Tie, X., and Bond, D. W.: Impacts of anthropogenic and natural NO_x sources over the U.S. on tropospheric chemistry, P. Natl. Acad. Sci. U.S.A, 100, 1505-1509, doi: 10.1073/pnas.252763799, 2003.

Zhao, B., Wang, S. X., Liu, H., Xu, J. Y., Fu, K., Klimont, Z., Hao, J. M., He, K. B., Cofala, J., and Amann, M.: NO_x emissions in China: historical trends and future perspectives, Atmos. Chem. Phys., 13, 9869-9897, doi: 10.5194/acp-13-9869-2013, 2013.

Zhao, Y., Qiu, L. P., Xu, R. Y., Xie, F. J., Zhang, Q., Yu, Y. Y., Nielsen, C. P., Qin, H. X., Wang, H. K., Wu, X. C., Li, W. Q., and Zhang, J.: Advantages of a city-scale emission inventory for urban air quality research and policy: the case of Nanjing, a typical industrial city in the Yangtze River Delta, China, Atmos. Chem. Phys., 15,

930   12623-12644, doi: 10.5194/acp-15-12623-2015, 2015.
931 Zong, Z., Wang, X., Tian, C., Chen, Y., Fang, Y., Zhang, F., Li, C., Sun, J., Li, J., and
932   Zhang, G.: First assessment of NO_x sources at a regional background site in North
933   China using isotopic analysis linked with modeling, Environ. Sci. Technol., 51, 5923-
934   5931, doi: 10.1021/acs.est.6b06316, 2017.

935

936

937

938

939

940

941

942

943

944

945

946
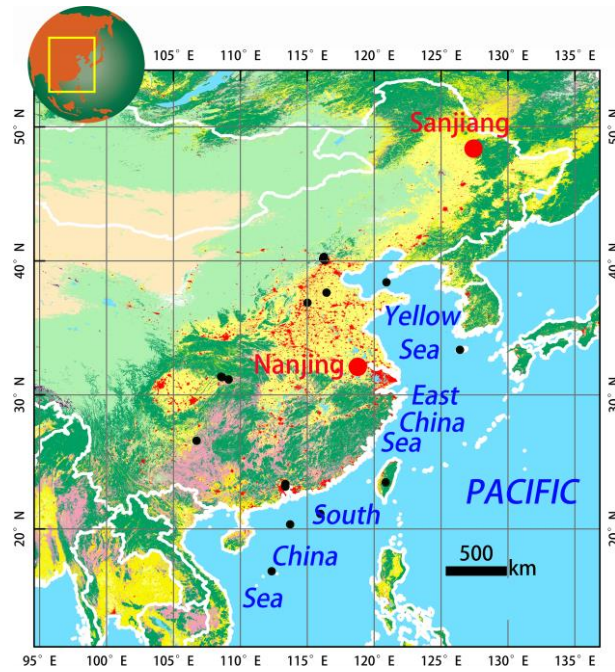
947

948   **Figure 1.** Location of the sampling sites Sanjiang and Nanjing. The black dots

949   indicate the location of sampling sites (sites are located in the area of mainland China

950   and the Yellow and East and South China Seas) with δ^{15}N-NO$_3^-$ data from the

951   literature (see also Table S4).

952

953

954

955

956

957

958
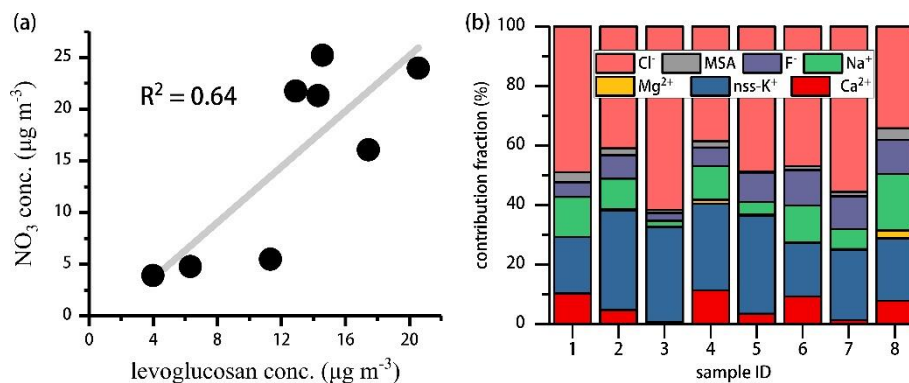
959

960 **Figure 2. (a)** Correlation analysis between the mass concentrations of levoglucosan

961 and aerosol nitrate during the Sanjiang sampling campaign; **(b)** Variation of fractions

962 of various inorganic species (MSA$^-$ stands for methyl sulphonate) during day-night

963 samplings at Sanjiang between 8 and October 2013 18 (sample ID 1 to 8,

964 respectively). The higher relative abundances of nss-K$^+$ and Cl$^-$ are indicative for a

965 biomass-burning dominated source. For sample ID information and exact sampling

966 dates, refer to Table S3.

967

968

969

970

971

972

973

974

975
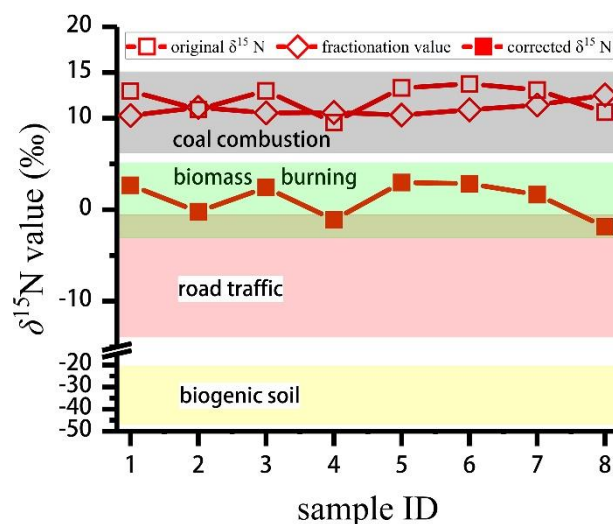
Figure 3. Original $\delta^{15}N$ values ($\delta^{15}N_{ini}$) for pNO$_3^-$, calculated values for the N isotope

fractionation (ε_N) associated with the conversion of gaseous NO$_x$ to pNO$_3^-$, and

corrected $\delta^{15}N$ values ($\delta^{15}N_{corr}$; $^{15}N_{ini}$ minus ε_N) of pNO$_3^-$ for each sample collected

during the Sanjiang sampling campaign. The colored bands represent the variation

range of $\delta^{15}N$ values for different NO$_x$ sources based on reports from the literature

(Table S2). See Table S3 for the information regarding sample ID.

982

983

984

985
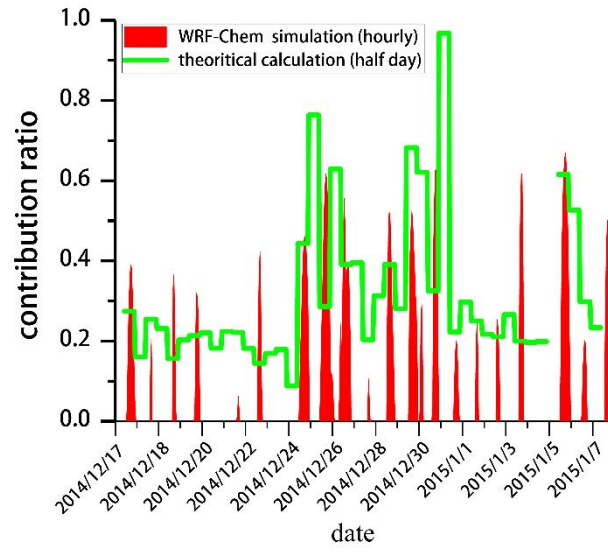
986

987 **Figure 4**. Comparison between the theoretical calculation and WRF-Chem simulation

988 of the average contribution ratio (γ) for nitrate formation in Nanjing via the reaction

989 of NO_2 and photochemically produced •OH.

990

991

992

993

994
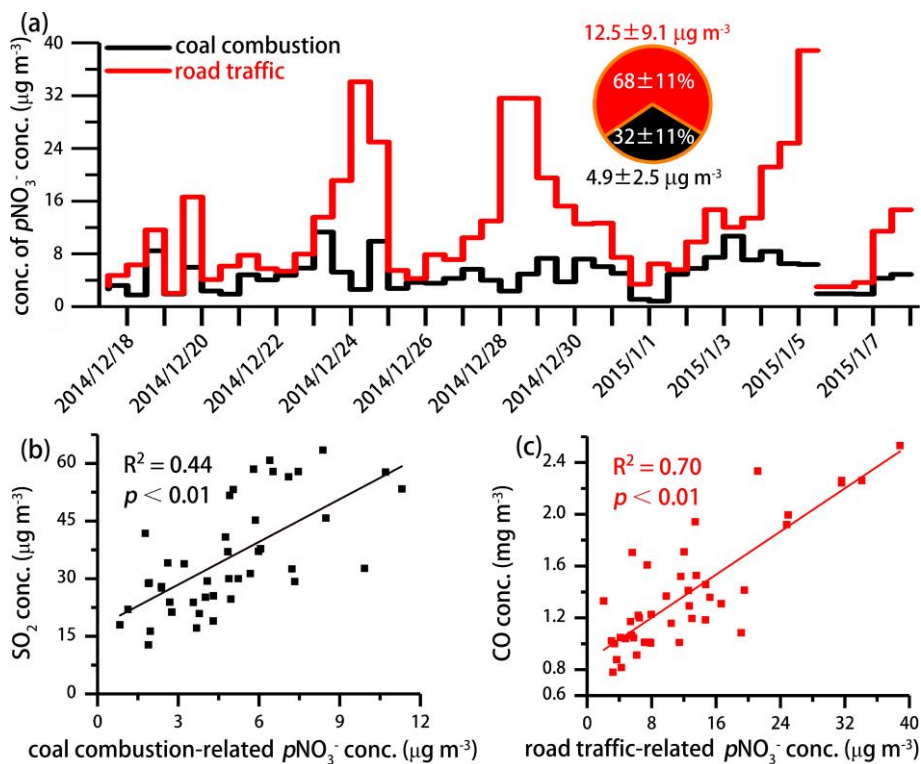
Figure 5. (**a**) Time-series variation of coal combustion and road traffic contribution to

the mass concentrations of ambient $p\mathrm{NO_3^-}$ in Nanjing, as estimated through MixSIR;

(**b**) Correlation analysis between the mass concentrations of coal combustion-related

$p\mathrm{NO_3^-}$ and SO_2; (**c**) Correlation analysis between the mass concentrations of road

traffic-related $p\mathrm{NO_3^-}$ and CO.
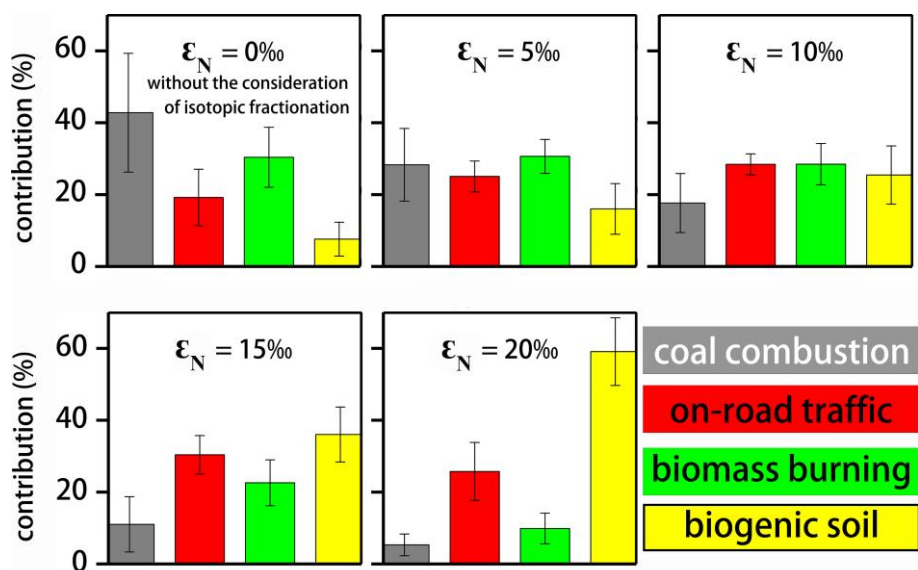
Figure 6. Estimates of the relative importance of single NO_x sources (mean $\pm$ 1σ) throughout China based on the original $\delta^{15}N\text{-}NO_3^-$ values extracted from the literature ($\varepsilon_N = 0‰$) and under consideration of significant N isotope fractionation during NO_x transformation ($\varepsilon_N = 5‰$, 10‰, 15‰ or 20‰).